International Journal of Minerals, Metallurgy and Materials
Volume 24, Number 7, July 2017, Page 842
DOI: 10.1007/s12613-017-1468-4

Phase transformation and crystal growth behavior of 8mol% ($SmO_{1.5}$, $GdO_{1.5}$, and $YO_{1.5}$) stabilized ZrO_2 powders

R. Mahendran, S.P. Kumaresh Babu, S. Natarajan, S. Manivannan, and A. Vallimanalan

Department of Metallurgical and Materials Engineering, National Institute of Technology, Tirchirappalli 620015, Tamil Nadu, India
(Received: 13 December 2016; revised: 20 January 2017; accepted: 15 February 2017)

Abstract: Nanocrystalline powders of ZrO_2–8mol%$SmO_{1.5}$ (8SmSZ), ZrO_2–8mol%$GdO_{1.5}$ (8GdSZ), and ZrO_2–8mol%$YO_{1.5}$ (8YSZ) were prepared by a simple reverse-coprecipitation technique. Differential thermal analysis/thermogravimetry (DTA/TG), Fourier transform infrared spectroscopy (FTIR), X-ray diffraction (XRD), Raman spectroscopy, and high-resolution transmission electron microscopy (HRTEM) were used to study the phase transformation and crystal growth behavior. The DTA results showed that the ZrO_2 freeze-dried precipitates crystallized at 529, 465, and 467°C in the case of 8SmSZ, 8GdSZ, and 8YSZ, respectively. The XRD and Raman results confirmed the presence of tetragonal ZrO_2 when the dried precipitates were calcined in the temperature range from 600 to 1000°C for 2 h. The crystallite size increased with increasing calcination temperature. The activation energies were calculated as 12.39, 12.45, and 16.59 kJ/mol for 8SmSZ, 8GdSZ, and 8YSZ respectively.

Keywords: zirconia; thermal analysis; reverse coprecipitation; activation energy

1. Introduction

The industrial applications of zirconia-based oxide ceramics include fuel cells, oxygen sensors, refractory materials, and thermal barrier coatings (TBCs). Zirconia has three polymorphs: at room temperature to 1400 K, it is monoclinic; the tetragonal phase is stable between 1400 and 2570 K; and the high-temperature phase, which is stable to its melting point, is cubic. The tetragonal and cubic phases can be retained at room temperature by doping ZrO_2 with different cations. Doping improves the mechanical and electrical properties of ZrO_2. Yttria is commonly used as a dopant at a concentration of 8mol% because the resulting doped zirconia (8YSZ) exhibits outstanding thermophysical and mechanical properties. However, 8YSZ cannot be used in long-term applications because it undergoes diffusion-controlled partitioning into tetragonal and cubic phases at temperatures above 1473 K. The tetragonal phase transforms to the monoclinic phase during cooling, accompanied by an increase in volume of 3%–5%. This volume change leads to the formation of cracks and results in the failure of coatings, thereby limiting the use of ZrO_2 as a structural material [1–3].

Rare-earth co-doped zirconia compositions have been studied as a potential replacement for conventional thermal barrier coating (TBC) materials. Numerous researchers have focused on using ZrO_2-based materials with added rare-earth oxide elements and with or without the addition of yttria for improving the phase stability; the additions of these oxide elements have resulted in nanostructured defect clusters, which reduce the thermal conductivity of TBC [3–9]. In recent years, the phase transformation and crystal growth behavior of nanocrystalline powders have become topics of interest for researchers because they strongly affect thermal barrier coating applications. Zhou *et al*. [10] synthesized 3YSZ, 5YSZ, 7YSZ, and 8YSZ powders via a coprecipitation technique and investigated the crystal growth behavior of powders using heat treated temperatures between 400 and 1200°C. They found that the activation energy was 7.65, 5.72, 5.77, and 5.76 kJ/mol at

Corresponding author: R. Mahendran E-mail: mahendran.meta@gmail.com

low temperatures from 400 to 800°C and that, at high temperatures, it increased abruptly to 25.34, 32.16, 32.76, and 34.30 kJ/mol, respectively. Kuo *et al.* [11] prepared 8YSZ, 9YSZ, and 10YSZ nanocrystalline powders by sol–gel and reported activation energies of 5.75, 4.22, and 5.24 kJ/mol, respectively. Chen *et al.* [12] reported the activation energy for 2YSZ nanoparticles as 34 kJ/mol. In addition, Lee *et al.* [13] obtained a crystallite growth activation energy of 7.26 kJ/mol for 8YSZ through a sol–gel process. The crystallization behavior of ZrO_2–$3Y_2O_3$–SrO nanosized powders were studied by Chu *et al.* [14]; their reported activation energies for the crystal growth of 1mol%, 2mol%, and 3mol% of SrO were 9.98, 9.04, and 7.43 kJ/mol, respectively.

Several techniques have been proven for producing TBC materials, including coprecipitation [10,15], hydrothermal processes [16–17], and sol–gel process [18–19]. Among these methods, coprecipitation is widely used to prepare nanocrystalline powders with shorter operating periods. Another advantage of coprecipitation over conventional methods is that it is a simple and inexpensive process [10].

In this study, 8mol%$SmO_{1.5}$–ZrO_2 (8SmSZ), 8mol%$GdO_{1.5}$–ZrO_2 (8GdSZ), and 8mol%$YO_{1.5}$–ZrO_2 (8YSZ) ceramic powders were synthesized by the chemical coprecipitation technique. The phase transformation and crystal growth behavior of synthesized powders heat-treated at different temperatures were investigated.

2. Experimental

The chemical coprecipitation technique was used to prepare ceramic powders. Zirconium oxychloride octahydrate ($ZrOCl_2{\cdot}8H_2O$), gadolinium nitrate hexahydrate ($Gd(NO_3)_3{\cdot}6H_2O$) and samarium nitrate hexahydrate ($Sm(NO_3)_3{\cdot}6H_2O$) were used as starting materials; they were dissolved in deionized water to form a 0.3 mol/L concentrated solution. Ammonium hydroxide (NH_4OH) was used as a precipitating agent. The mixed solution was slowly added dropwise to the NH_4OH solution. The resultant solution was magnetically stirred, and its pH value was maintained between 10 and 11. During the process of ammonia addition, white precipitates gradually formed. The white precipitates were filtered and washed several times with deionized water and ethanol. The precipitates were then dried in an oven at 100°C for 5 h. The powder mixture was ground in an agate mortar and then calcined at different temperatures for determination of the phase transformation and activation energy.

2.1. Characterization of the powders

Thermal analysis was carried out on the as-prepared dried precipitates using a simultaneous thermal analyzer (STA 8000, Perkin Elmer); the samples were heated under a nitrogen atmosphere at a heating rate of 5°C/min. FTIR (Spectrum-II, Perkin Elmer) was used to characterize the as-prepared dried precipitates and calcined samples (600°C) over the wavenumber range from 1000 to 4000 cm^{-1}. The phase analysis of the calcined powders was carried out by X-ray powder diffraction (XRD; Rigaku Ultima III) with Cu K_α radiation (λ = 0.15406 nm) at a scanning rate of 2°/min and a step size of 0.05° over the scanning range from 20° to 80°. The average crystallite size (D_t) of the ceramic powders was determined from broadening of the (011) diffraction line of the tetragonal phase. It was calculated using the Scherrer equation (Eq. (1)) [10–11]:

$$D_t = \frac{0.89\lambda}{\beta\cos\theta} \quad (1)$$

where D_t, λ, β, and θ are the crystallite size of the tetragonal phase, the wavelength of the Cu K_α radiation, the corrected full-width at half-maximum (FWHM), and the Bragg angle of the (011) reflection of the tetragonal phase, respectively. Micro-Raman spectroscopy (Labram HR Evolution, Horiba Jobin Yvon) was conducted; the spectra were recorded for the calcined powders in the spectrum range of 100 to 700 cm^{-1} at room temperature. An Nd:YAG laser was used as an excitation source. The microstructure of the calcined powders was observed by high-resolution transmission electron microscopy (HRTEM; JEOL, JEM 2100).

3. Results and discussion

3.1. Thermal and FTIR analyses

Fig. 1 shows the DTA/TG curves of 8SmSZ, 8GdSZ, and 8YSZ samples dried at 100°C. The TG curve in Fig. 1(a) shows two weight losses. The first stage is associated with the evaporation of water and ammonia present in the dried precipitates (30 to 220°C), with a weight loss of 17%. A second weight loss of 4% was observed and attributed to the decomposition of zirconium hydroxide formed during the precipitation process with increasing annealing temperature. The peak at 529°C in the DTA curve indicates the formation of nanocrystalline zirconia.

The curves in Fig. 1(b), showing a weight loss of 22% and a crystallization temperature of 465°C, are similar to those of 8SmSZ in Fig. 1(a). In the case of 8YSZ (Fig. 1(c)), a weight loss of 25% occurs between the temperature range from 30 to 467°C and a peak at 467°C in the DTA curve indicates the formation of a crystalline phase. In a previous report, Wang *et al.* [20] reported that the transformation of nanocrystalline zirconia from ZrOH occurs near 470°C for the precipitation process.

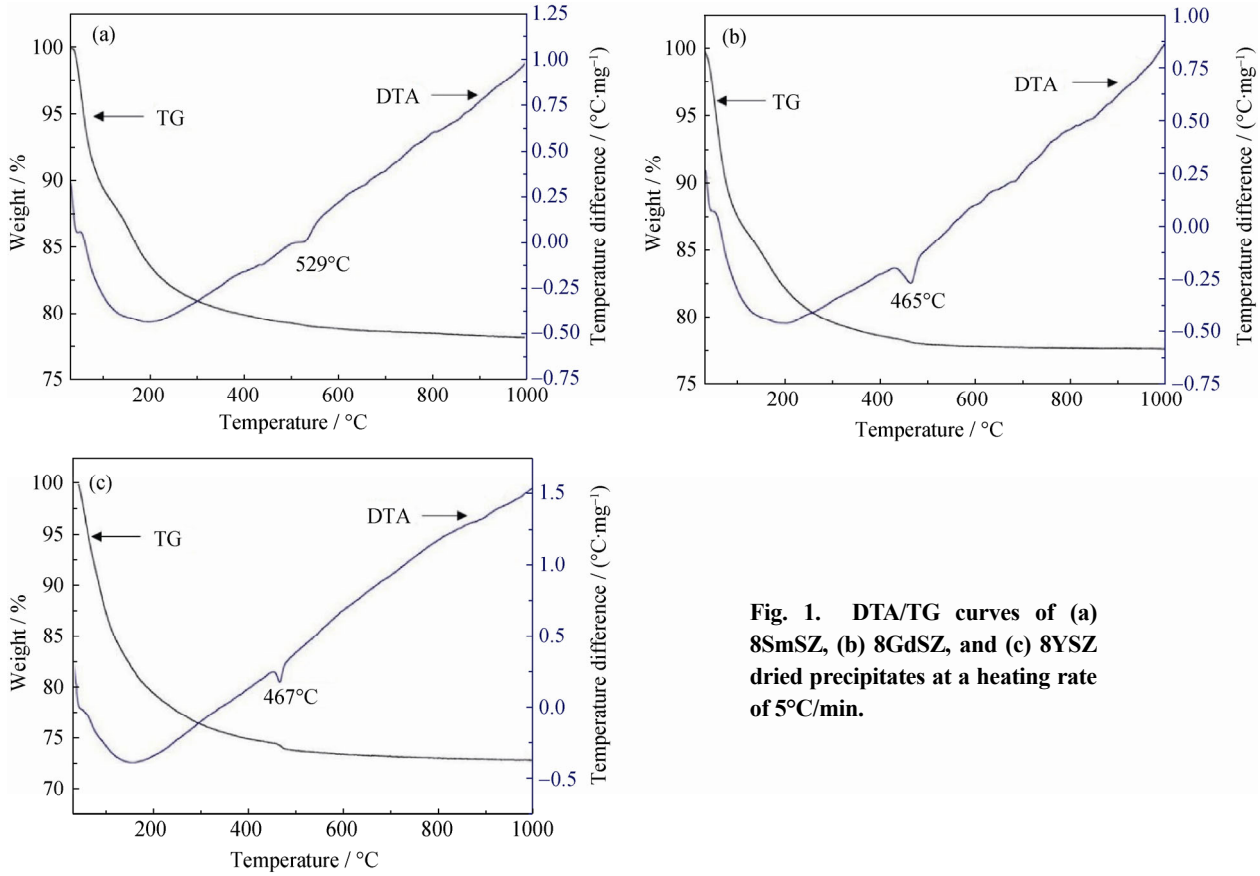

Fig. 1. DTA/TG curves of (a) 8SmSZ, (b) 8GdSZ, and (c) 8YSZ dried precipitates at a heating rate of 5°C/min.

The FT-IR spectra of the dried precipitates and samples calcined at 600°C are shown in Fig. 2. In Fig. 2(a), the bands appearing at 1548 and 1332 cm^{-1} are attributed to the N–O asymmetrical stretches in N–O [21–22] and to –OH, respectively. Another band at 1631 cm^{-1} arises from the H–O–H bending bonds [13]. In all cases, the wide peak at 3349 cm^{-1} corresponds to O–H stretching; the wide nature of this peak is associated with hydrogen-bonded chains [23–24]. The FTIR spectra of powders calcined at 600°C for 2 h are shown in Fig. 2(b). The characteristic O–H bands disappeared, and other less-intense bands appeared with increasing heat-treatment temperature.

3.2. Phase development of ZrO_2-doped powders after calcination

The XRD patterns of as-prepared powder samples of 8SmSZ, 8GdSZ, and 8YSZ calcined at different temperatures for 2 h are shown in Figs. 3(a), 3(b), and 3(c), respectively. At the lowest temperature (300°C), the samples were amorphous; after calcination at 600°C, the samples were

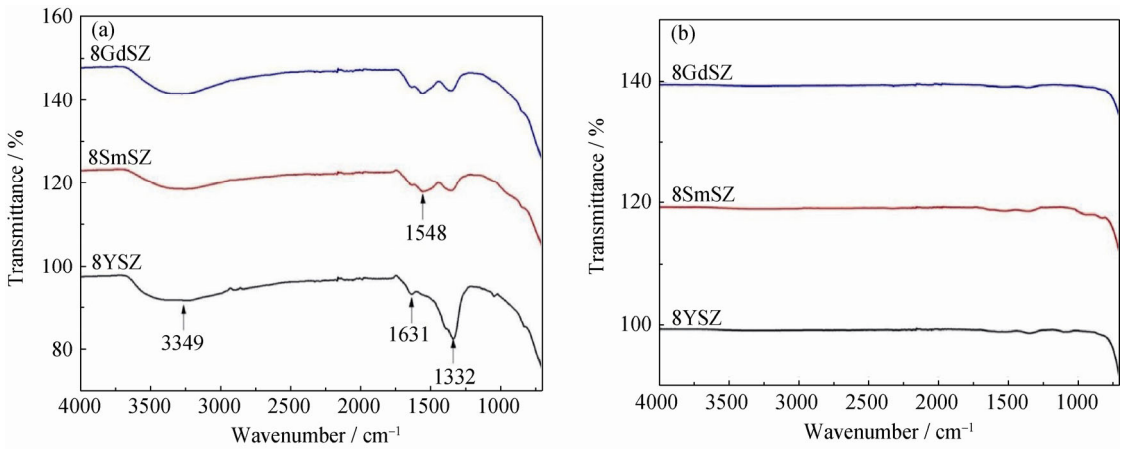

Fig. 2. FTIR spectra of 8YSZ, 8GdSZ, and 8SmSZ dried precipitates (a) and the samples calcined at 600°C for 2 h (b).

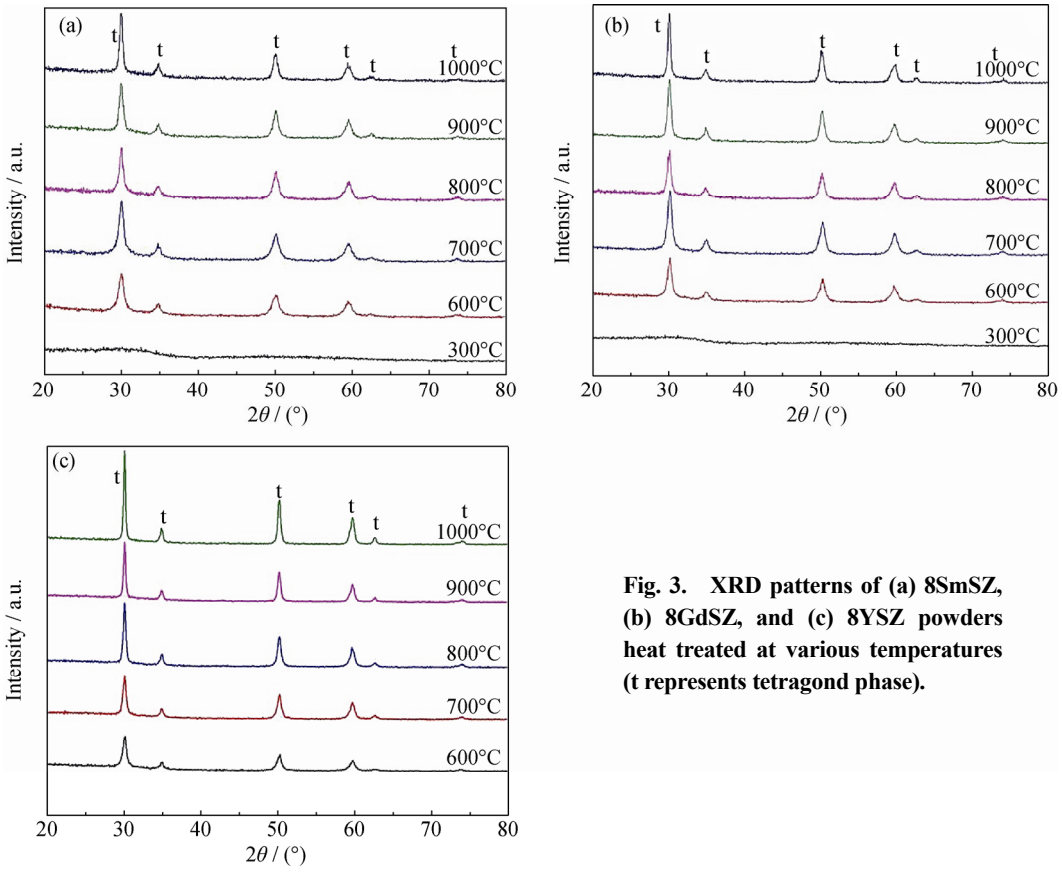

Fig. 3. XRD patterns of (a) 8SmSZ, (b) 8GdSZ, and (c) 8YSZ powders heat treated at various temperatures (t represents tetragond phase).

completely crystallized, and a broad pattern was observed in all cases. The (011), (110), (020), (121), (022), and (220) peaks correspond to tetragonal zirconia, indicating that dopants had been dissolved into ZrO_2 crystals and that no other phases were present. When the calcination temperature was increased to 1000°C, the reflection peaks of the tetragonal phase became sharper and stronger. A decrease in FWHM and an increase in nanocrystallites' size occurred in all cases as a result of increasing calcination temperature [10,25]. The Raman spectra, which are shown in Fig. 4, also confirm the single tetragonal phase. The monoclinic phase is the most thermodynamically stable phase at room temperature for undoped ZrO_2 because it favors 7-fold coordination. Partial substitution of lower-valent atoms such as Sm^{3+}, Gd^{3+}, or Y^{3+} would create oxygen vacancies in the ZrO_2 lattice for charge compensation. According to kinetics, ZrO_2 favors 7-fold coordination; meanwhile, because of the larger ionic radii of the dopants, the created oxygen vacancies tend to associate with Zr^{4+}. Hence, ZrO_2 changes the lattice structure to 8-fold coordination, which leads to the formation of the tetragonal structure [25–27]. The tetragonal-to-monoclinic phase transformation is a size-dependent transformation [28], and the critical crystallite size for the transformation to occur has been calculated as 30 nm [29]. These results are consistent with the previous discussions because the crystallite size of ZrO_2 doped with various dopants is well below 30 nm; thus, the tetragonal-to-monoclinic phase transformation did not occur.

3.3. Raman spectral analysis

The Raman spectra of 8SmSZ calcined at 600, 700, and 900°C, 8GdSZ calcined at 600 and 700°C, and 8YSZ calcined at 800°C are shown in Fig. 4. The five peaks at (1)

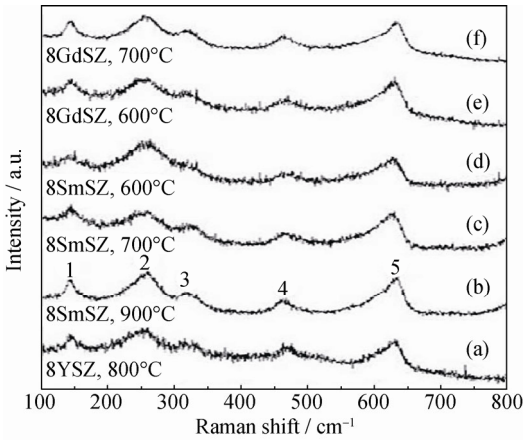

Fig. 4. Raman spectra of (a) 8YSZ, 800°C, (b) 8SmSZ, 900°C, (c) 8SmSZ, 700°C, (d) 8SmSZ, 600°C, (e) 8GdSZ, 600°C, and (f) 8GdSZ, 700°C.

143 cm^{-1}, (2) 257 cm^{-1}, (3) 322 cm^{-1}, (4) 465 cm^{-1}, and (5) 638 cm^{-1} are Raman modes of t-ZrO_2 [18,30–31]. No vibration modes corresponding to the monoclinic phase were observed, consistent with the XRD results. The mode at E_g (142) is the mode of Zr–O–Zr and O–Zr–O bending, those at E_g (260), E_g (467), and B_{1g} (638) are the modes of Zr–O stretching, and that at B_{1g} (322) is the Zr–O bending mode. Raman shifts were observed in the spectra of all the doped samples because of the lattice disorder and the lattice strain developed within crystals as a result of the substitution of cations [32–33].

3.4. Crystal growth behavior of doped ZrO_2 powders

The average crystallite size of various doped ZrO_2 powders calcined at temperatures from 600 to 1000°C for 2 h is shown in Fig. 5(a). The average crystallite size was calculated by the Scherrer equation; and the results are listed in Table 1. An increase in calcination temperature was found to increase the crystallize size in all of the doped samples. We observed that the crystallite size of 8SmSZ was the smallest, whereas that of 8YSZ was the largest. Initially, in the case of 8SmSZ, calcination at a temperature of 600 to 800°C resulted in an increase of the crystallite size from 9 to 12 nm. When the calcination temperature was further increased to 1000°C, the crystallite size reached a value of 16.83 nm; this increase was attributed to the effect of heat-treatment temperature on crystal growth [10,18]. By contrast, the average crystallite size of 8YSZ increased from 13.97 to 20.17 nm as the calcination temperature was increased from 600 to 800°C and then increased to 28.15 nm when the calcination temperature was increased to 1000°C. A similar trend was observed for 8GdSZ, where the crystallite size increased from 12.13 to 14.69 nm at low temperatures and then to 21.29 nm at 1000°C.

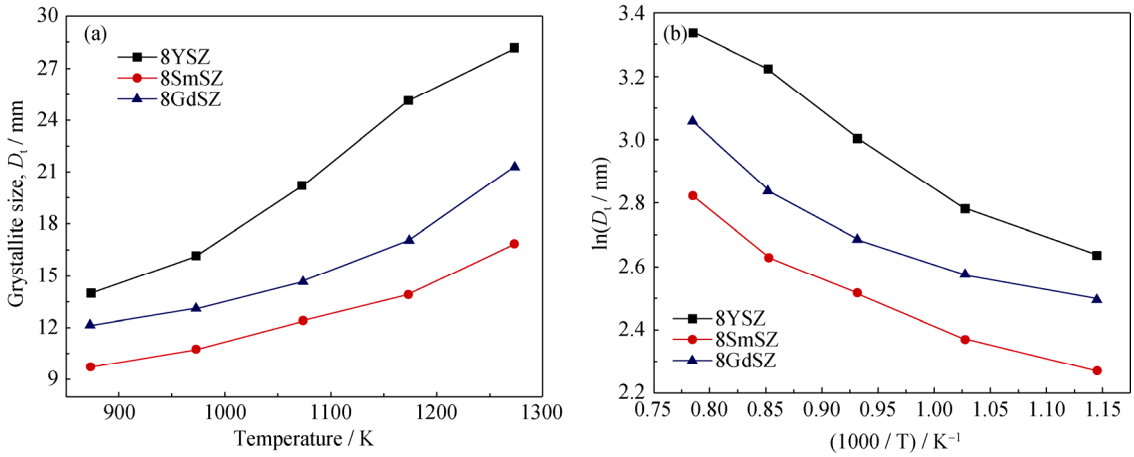

Fig. 5. Relation between average crystallite size and heat-treatment temperature (a) and lnD_t vs. 1/T (b).

Table 1. Average crystallite sizes of nanopowders heat-treated at various temperatures for 2 h and the corresponding activation energy for crystal growth

Temperature / °C	Average crystallite size of doped ZrO_2 nanopowders / nm		
	8YSZ	8SmSZ	8GdSZ
600	13.97	9.68	12.13
700	16.14	10.71	13.12
800	20.16	12.37	14.69
900	25.14	13.88	17.06
1000	28.15	16.83	21.29
Activation energy / (kJ·mol^{-1})	16.95	12.45	12.39

The activation energy for crystal growth was calculated by the Arrhenius equation:

$$D_t = k\exp\left(\frac{\Delta E}{RT}\right) \quad (2)$$

where D_t is the average crystallite size estimated from Eq. (1), k is a constant, R is the ideal gas constant, T is the heat-treatment temperature, and ΔE is the activation energy.

Taking the natural logarithm of both sides of Eq. (2) gives

$$\ln D_t - \ln k = -\Delta E/(RT) \quad (3)$$

Therefore, the activation energy for crystal growth of various doped nanocrystalline zirconia powders was determined from a linear fitting of a plot of the logarithm of the average crystallite size versus the reciprocal of the heat-treatment temperature, as shown in Fig. 5(b). The activation energies of 8YSZ, 8SmSZ, and 8GdSZ for the crystal growth of doped samples, as calculated from Eq. (3), are 16.95, 12.39, and 12.46 kJ/mol, respectively. On the basis of previous works, the activation energies obtained in this work were lower than the result of 13 kJ/mol [25] in the cases of 8SmSZ and 8GdSZ and the results of 34 [12], 29.2 [34], and 24.79 kJ/mol [35] reported for 8YSZ. The lower activation energies in the present work are associated with the presence of a large amount of oxygen-ion vacancies within the nanocrystalline lattices [25]. A large number of oxygen vacancies can be created in nanocrystalline powders via two different mechanisms: (1) doping with lower-valence atoms such as Sm^{3+}, Gd^{3+}, and Y^{3+} can create huge oxygen vacancies and (2) the concentration of oxygen vacancies can increase in nanocrystalline ceramic particles when the nanoparticle size is less than 20 nm [10,25]. These combined effects increase the number of oxygen vacancies, which reduces the activation energy for the crystal growth in the present study.

3.5. Microstructure of doped ZrO_2 powders after calcination

Figs. 6(a), 6(c), and 6(e) show the bright-field TEM images of 8SmSZ, 8GdSZ, and 8YSZ, respectively, which reveal that the particles are agglomerated and crystallized. Figs. 6(b), 6(d), and 6(f) show the corresponding SAED patterns of 8SmSZ, 8GdSZ, and 8YSZ. The SAED patterns confirmed the existence of single-phase tetragonal ZrO_2, consistent with the XRD results.

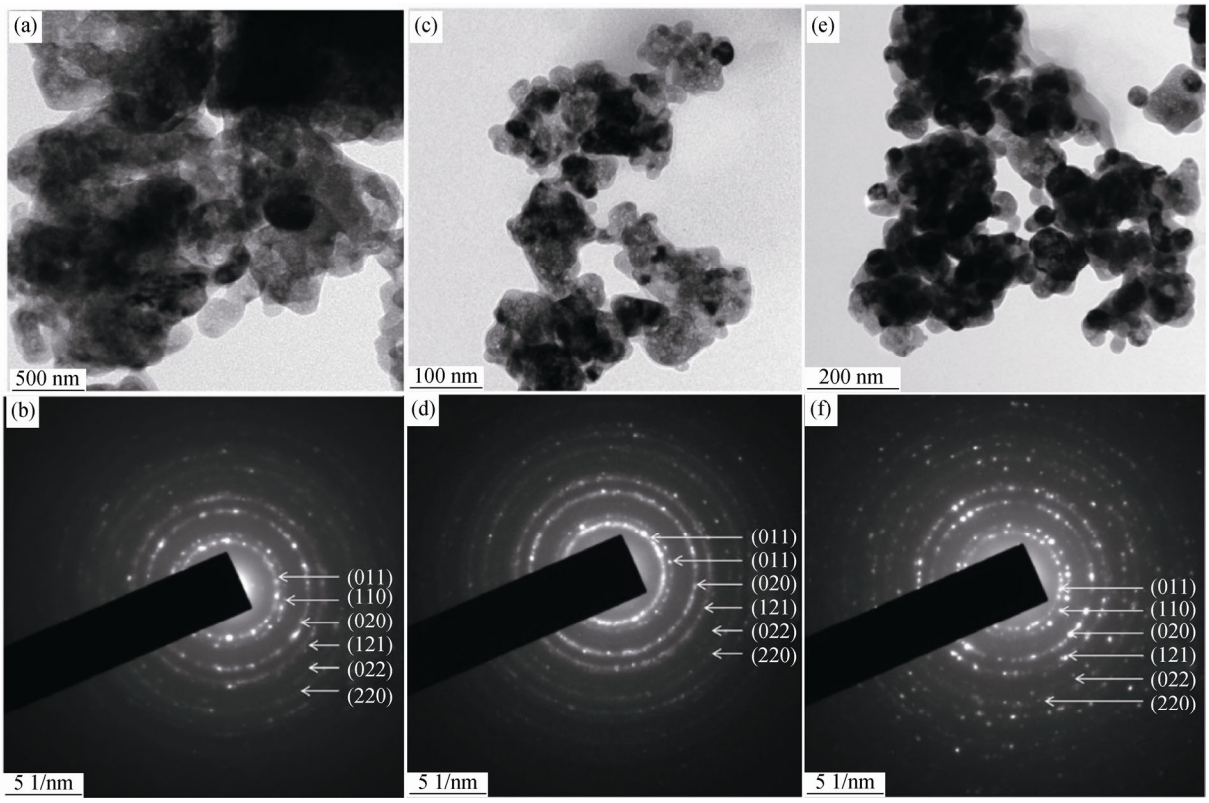

Fig. 6. HRTEM micrographs and the corresponding SAED patterns of doped samples calcined at 800°C for 2 h: (a) bright-field image of 8SmSZ; (b) SAED pattern of 8SmSZ; (c) bright-field image of 8GdSZ; (d) SAED pattern of 8GdSZ; (e) bright-field image of 8YSZ; (f) SAED pattern of 8YSZ.

4. Conclusion

Nanocrystalline 8SmSZ, 8GdSZ, and 8YSZ powders were synthesized by the coprecipitation technique. The DTA results indicate that nanocrystalline tetragonal zirconia crystallized at 529°C for 8SmSZ, at 465°C for 8GdSZ, and at 467°C for 8YSZ. The XRD results confirmed that ZrO_2 was present as tetragonal-phase ZrO_2. It exhibited excellent phase stability, and the crystallite size increased when the samples were calcined at temperatures between 600 and 1000°C. The activation energies for the crystal growth of 8SmSZ, 8GdSZ, and 8YSZ nanocrystalline tetragonal zirconia were calculated as 12.45, 12.35, and 16.95 kJ/mol, respectively. The SAED patterns also confirmed the presence of tetragonal zirconia.

References

[1] N.P. Padture, M. Gell, and E.H. Jordan, Thermal barrier coatings for gas-turbine engine applications, *Science*, 296(2002), No. 5566, p. 280.

[2] D.R. Clarke, M. Oechsner, and N.P. Padture, Thermal-barrier coatings for more efficient gas-turbine engines, *MRS Bull.*, 37(2012), No. 10, p. 891.

[3] Y.L. Zhang, L. Guo, Y.P. Yang, H.B. Guo, H.J. Zhang, and S.K. Gong, Influence of Gd_2O_3 and Yb_2O_3 Co-doping on phase stability, thermo-physical properties and sintering of 8YSZ, *Chin. J. Aeronaut.*, 25(2012), No. 6, p. 948.

[4] J. Feng, X.R. Ren, X.Y. Wang, R. Zhou, and W. Pan, Thermal conductivity of ytterbia-stabilized zirconia, *Scripta Mater.*, 66(2012), No. 1, p. 41.

[5] L.L. Sun, H.B. Guo, H. Peng, S.K. Gong, and H.B. Xu, Influence of partial substitution of Sc_2O_3 with Gd_2O_3 on the phase stability and thermal conductivity of Sc_2O_3-doped ZrO_2, *Ceram. Int.*, 39(2013), No. 3, p. 3447.

[6] H.F. Liu, S.L. Li, Q.L. Li, and Y.M. Li, Investigation on the phase stability, sintering and thermal conductivity of Sc_2O_3–Y_2O_3–ZrO_2 for thermal barrier coating application, *Mater. Des.*, 31(2010), No. 6, p. 2972.

[7] Q.L. Li, X.Z. Cui, S.Q. Li, W.H. Yang, C. Wang, and Q. Cao, Synthesis and phase stability of scandia, gadolinia, and ytterbia Co-doped zirconia for thermal barrier coating application, *J. Therm. Spray Technol.*, 24(2015), No. 1, p. 136.

[8] D.M. Zhu, Y.L. Chen, and R.A. Miller, Defect clustering and nanophase structure characterization of multi-component rare earth-oxide-doped zirconia–yttria thermal barrier coatings, *Ceram. Eng. Sci. Proc.*, 24(2003), No. 3, p. 525.

[9] M.B. Ponnuchamy and A.S. Gandhi, Phase and fracture toughness evolution during isothermal annealing of spark plasma sintered zirconia co-doped with Yb, Gd and Nd oxides, *J. Eur. Ceram. Soc.*, 35(2015), No. 6, p. 1879.

[10] Y.J. Zhou, W.H. Yuan, Q.L. Huang, W.Z. Huang, H.F. Cheng, and H.T. Liu, Effect of Y_2O_3 addition on the phase composition and crystal growth behavior of YSZ nanocrystals prepared via coprecipitation process, *Ceram. Int.*, 41(2015), No. 9, p. 10702.

[11] C.W. Kuo, Y.H. Shen, I.M. Hung, S.B. Wen, H.E. Lee, and M.C. Wang, Effect of Y_2O_3 addition on the crystal growth and sintering behavior of YSZ nanopowders prepared by a sol–gel process, *J. Alloys Compd.*, 472(2009), No. 1-2, p. 186.

[12] S.G. Chen, Y.S. Yin, D.P. Wang, and J. Li, Reduced activation energy and crystalline size for yttria-stabilized zirconia nano-crystals: an experimental and theoretical study, *J. Cryst. Growth*, 267(2004), No. 1-2, p. 100.

[13] Y.H. Lee, C.W. Kuo, I.M. Hung, K.Z. Fung, and M.C. Wang, The thermal behavior of 8mol% yttria-stabilized zirconia nanocrystallites prepared by a sol–gel process, *J. Non-Cryst. Solids*, 351(2005), No. 49, p. 3709.

[14] H.L. Chu, W.S. Hwang, J.K. Du, K.K. Chen, and M.C. Wang, Effect of SrO addition on the growth behavior of ZrO_2–$3Y_2O_3$ precursor powders synthesized by a coprecipitation process, *Ceram. Int.*, 42(2016), No. 8, p. 10251.

[15] A. Loganathan and A.S. Gandhi, Fracture toughness of t' ZrO_2 stabilised with $MO_{1.5}$ (M =Y, Yb & Gd) for thermal barrier application, *Trans. Indian Inst. Met.*, 64(2011), No. 1, p. 71.

[16] Y.B. Khollam, A.S. Deshpande, A.J. Patil, H.S. Potdar, S.B. Deshpande, and S.K. Date, Synthesis of yttria stabilized cubic zirconia (YSZ) powders by microwave-hydrothermal route, *Mater. Chem. Phys.*, 71(2001), No. 3, p. 235.

[17] Isabel Gonzalo, B. Ferrari, and M.T. Colomer, Influence of the urea content on the YSZ hydrothermal synthesis under dilute conditions and its role as dispersant agent in the post-reaction medium, *J. Eur. Ceram. Soc.*, 29(2009), No. 15, p. 3185.

[18] Q.L. Huang, W.H. Yuan, W.Z. Huang, H.F. Cheng, Y.J. Zhou, and H.T. Liu, Effect of organic additions on the phase composition and crystal growth behavior of 8wt% yttria-stabilized zirconia nanocrystals prepared via sol–gel process, *J. Sol-Gel Sci. Technol.*, 74(2015), No. 2, p. 432.

[19] C. Suciu, A.C. Hoffmann, A. Vik, and F. Goga, Effect of calcination conditions and precursor proportions on the properties of YSZ nanoparticles obtained by modified sol–gel route, *Chem. Eng. J.*, 138(2008), No. 1-3, p. 608.

[20] J.A. Wang, M.A. Valenzuela, J. Salmones, A. Vázquez, A. Garcia-Ruiz, and X. Bokhimi, Comparative study of nanocrystalline zirconia prepared by precipitation and sol–gel methods, *Catal. Today*, 68(2001), No. 1-3, p. 21.

[21] P.K. Sharma, R. Nass, and H. Schmidt, Effect of solvent, host precursor, dopant concentration and crystallite size on the fluorescence properties of Eu(III) doped yttria, *Opt. Mater.*, 10(1998), No. 2, p. 161.

[22] K. Richardson and M. Akinc, Preparation of spherical yttrium oxide powders using emulsion evaporation, *Ceram. Int.*, 13(1987), No. 4, p. 253.

[23] T. Lopez, E. Sanchez, P. Bosch, Y. Meas, and R. Gomez, FTIR and UV-Vis (diffuse reflectance) spectroscopic characterization of TiO_2 sol–gel, *Mater. Chem. Phys.*, 32(1992), No. 2, p. 141.

[24] H.E. Lee, J.K. Du, Y.Y. Sie, C.H. Wang, J.H. Wu, C.L. Wang, W.S. Hwang, H.H. Huang, W.L. Li, and M.C. Wang, Thermal properties and phase transformation of 2mol% Y_2O_3–PSZ nanopowders prepared by a Co-precipitation process, *J. Non-Cryst. Solids*, 357(2011), No. 10, p. 2103.

[25] S. Shukla, S. Seal, R. Vij, and S. Bandyopadhyay, Reduced activation energy for grain growth in nanocrystalline yttria-stabilized zirconia, *Nano Lett.*, 3(2003), No. 3, p. 397.

[26] S.M. Ho, On the structural chemistry of zirconium oxide, *Mater. Sci. Eng.*, 54(1982), No. 1, p. 23.

[27] Y.W. Hsu, K.H. Yang, K.M. Chang, S.W. Yeh, and M.C. Wang, Synthesis and crystallization behavior of 3mol% yttria stabilized tetragonal zirconia polycrystals (3Y–TZP) nanosized powders prepared using a simple co-precipitation process, *J. Alloys Compd.*, 509(2011), No. 24, p. 6864.

[28] T. Chraska, A.H. King, and C.C. Berndt, On the

size-dependent phase transformation in nanoparticulate zirconia, *Mater. Sci. Eng. A*, 286(2000), No. 1, p. 169.

[29] R.C. Garvie, R.H. Hannink, and R.T. Pascoe, Ceramic steel?, *Nature*, 258(1975), p. 703.

[30] D.J. Kim, H.J. Jung, and I.S. Yang, Raman spectroscopy of tetragonal zirconia solid solution, *J. Am. Ceram. Soc.*, 76(1993), No. 8, p. 2106.

[31] L. Qu and K.L. Choy, Thermophysical and thermochemical properties of new thermal barrier materials based on Dy_2O_3–Y_2O_3 co-doped zirconia, *Ceram. Int.*, 40(2014), No. 8, p. 11593.

[32] X.Q. Niu, M. Xie, F. Zhou, R.D. Mu, X.W. Song, and S.L. An, Substituent influence of yttria by gadolinia on the tetragonal phase stability for Y_2O_3–Ta_2O_5–ZrO_2 ceramics at 1300°C, *J. Mater. Sci. Technol.*, 30(2014), No. 4, p. 381.

[33] A.M. Limarga, J. Iveland, M. Gentleman, D.M. Lipkin, and D.R. Clarke, The use of Larson-Miller parameters to monitor the evolution of Raman lines of tetragonal zirconia with high temperature aging, *Acta Mater.*, 59(2011), No. 3, p. 1162.

[34] C.H. Wang, M.C. Wang, J.K. Du, Y.Y. Sie, C.S. Hsi, and H.E. Lee, Phase transformation and nanocrystallite growth behavior of 2mol% yttria-partially stabilized zirconia (2Y–PSZ) powders, *Ceram. Int.*, 39(2013), No. 5, p. 5165.

[35] C.W. Kuo, K.C. Lee, F.L. Yen, Y.H. Shen, H.E. Lee, S.B. Wen, M.C. Wang, and M.M. Stack, Growth kinetics of tetragonal and monoclinic ZrO_2 crystallites in 3mol% yttria partially stabilized ZrO_2 (3Y–PSZ) precursor powder, *J. Alloys Compd.*, 592(2014), p. 288.